Deterministic Preparation of Optical Squeezed Cat and Gottesman-Kitaev-Preskill States

Matthew S. Winnel[*], Joshua J. Guanzon, Deepesh Singh, and Timothy C. Ralph

Centre for Quantum Computation and Communication Technology, School of Mathematics and Physics,
University of Queensland, St Lucia, Queensland 4072, Australia

Large-amplitude squeezed cat states and high-quality Gottesman-Kitaev-Preskill (GKP) states are essential for effective quantum error correction, yet their optical preparation has been hindered by challenges such as low success probabilities, small amplitudes, and insufficient squeezing. Addressing these limitations, our research introduces scalable optical schemes for the deterministic preparation of large-amplitude squeezed cat states from photon-number states. Fock states have the benefit of producing consistent cat states across all measurement outcomes and intrinsically provides a degree of squeezing. Notably, these squeezed cat states facilitate the deterministic generation of high-quality approximate GKP states via "breeding," showing that GKP error correction in optics is technically feasible in near-term experiments. Our schemes allow fault-tolerant quantum computation through the use of GKP error correction.

Introduction.—To harness the potential benefits of quantum technologies for real-world applications [1,2], it is crucial to address the challenge of noise [3]. Among the diverse strategies for redundantly encoding quantum information, continuous variable [4–8] systems stand out for their ability to utilize the infinite-dimensional Hilbert space of quantum oscillators.

Achieving large-amplitude cat [9–14] and high-quality Gottesman-Kitaev-Preskill (GKP) states [15] in optical systems presents a significant challenge [16,17]. Historically, the generation of cat states primarily utilized Gaussian squeezed-vacuum states combined with conditional photon-number measurements executed on a beam splitter [18]. This method, despite marking considerable experimental advances [19,20], tends to yield states characterized by low amplitude, insufficient squeezing, or a high degree of nondeterminism [21–28].

In this Letter, we address the challenges associated with preparing large-amplitude squeezed cat states and demonstrate two methods to achieve this with a high probability of success.

Our two schemes deterministically produce approximate squeezed cat states with a random but known phase angle ϕ and approximately constant amplitude, attributable to the use of an n-photon Fock state with a fixed amplitude as the input. To achieve a fully deterministic state preparation, a passive phase rotation can be applied to the generated cat states (or this rotation may be tracked in software).

Our first scheme offers a deterministic approach for transforming large Fock states into large-amplitude squeezed cat states. Acknowledging the challenges in generating large Fock states [29–35], our second scheme provides an alternative strategy for preparing cat states. Our second scheme efficiently converts squeezed Fock states (or any state with even or odd photon-number parity) into cat states, which are simpler to produce experimentally. While using smaller n values introduces some nondeterminism—resulting in not all states achieving high fidelity—this can be advantageous. It enables selective generation of large-amplitude cat states from smaller Fock states, enhancing the versatility of scheme II for producing high-quality cat states in experimental settings.

Among the promising avenues explored for the realization of optical GKP states, nondeterministic preparation methods have been proposed, notably utilizing "Gaussian boson sampling"-like devices [36–40]. However, the most straightforward strategy for deterministically preparing GKP states involves the "breeding" of large-amplitude squeezed cat states [41–43]. By enabling reliable and deterministic generation of large-amplitude squeezed cat states, our work paves the way for universal fault-tolerant quantum computation [44] using GKP error correction.

The recent work by Ref. [45] employs a nondeterministic approach to generate propagating GKP states. This development aligns with the lower-order implementation of our proposed schemes, thereby reinforcing the technical viability and near-term feasibility of our approach.

We validate our analytical results through numerical simulations in the Fock basis, limiting the dimensionality of the Fock space to a manageable size while ensuring accuracy and validity of our simulations. We provide our code [46,47] in [48,49].

Preliminaries.—Our aim is to deterministically prepare squeezed cats of the form

$$|\mathcal{C}_{\alpha,r}^{\pm}\rangle \equiv \mathcal{N}(|\alpha, r\rangle \pm |-\alpha, r\rangle), \qquad (1)$$
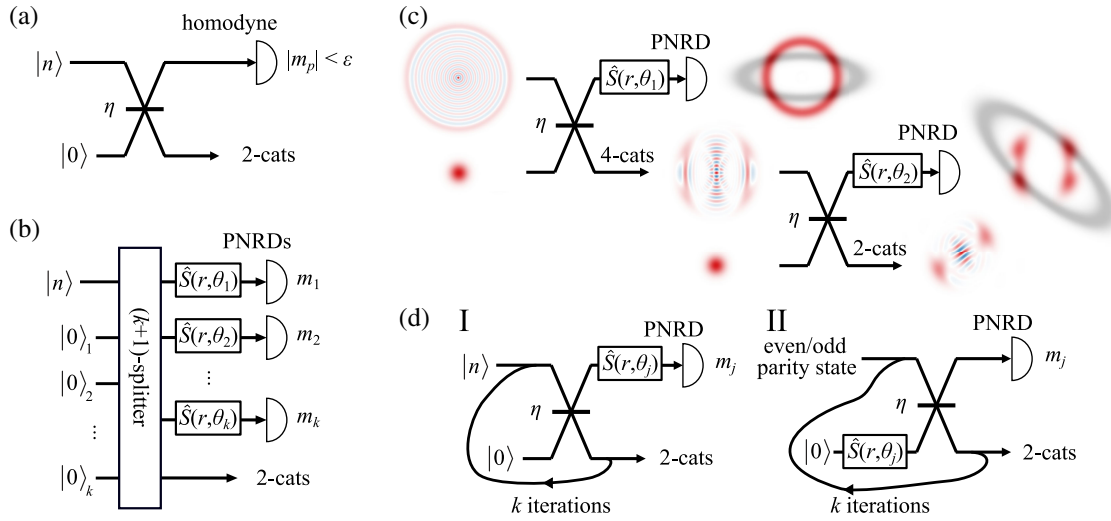
FIG. 1. Optical circuits of large-amplitude squeezed cat state preparation. (a) Illustrates the nondeterministic approach from Ref. [23] where a Fock state $|n\rangle$ is combined with a vacuum state on a beam splitter characterized by a transmissivity $\eta = 1/2$, homodyne detection of one output mode is performed and squeezed cat states are prepared in the other mode, dependent upon the measurement outcome being near zero. (b) Depicts our deterministic preparation method. A Fock state undergoes division through a $(k + 1)$ splitter, followed by squeezing operations in varying directions θ_j, and is subjected to photon-number-resolving detection (PNRDs). This process guarantees the deterministic generation of a squeezed cat state in the remaining mode, given a sufficiently large initial n. (c) Presents Wigner functions to illustrate the operational principle of the scheme for $k = 2$. (d) Showcases two iterative schemes designed for the preparation of squeezed cat states.

where $|\alpha, r\rangle \equiv \hat{D}(\alpha)\hat{S}(r)|0\rangle$ is a displaced squeezed vacuum state in the position-quadrature direction, α is real, and $\mathcal{N}$ is the normalization constant. The $+$ and $-$ superpositions consist of only even or odd photon numbers, respectively. The displacement and squeezing operators are defined as $\hat{D}(\alpha) \equiv e^{\alpha\hat{a}^\dagger - \alpha^*\hat{a}}$ and $\hat{S}(r, \theta) \equiv e^{(r/2)(\hat{a}^2 e^{-2i\theta} - \hat{a}^{\dagger 2} e^{2i\theta})}$, respectively. For squeezing ($r > 0$) and antisqueezing ($r < 0$) we write $\hat{S}(r) \equiv \hat{S}(r, \theta = 0)$.

Gaussian operations such as squeezing and rotations can transform squeezed cats into the form of Eq. (1). The phase rotation operator is $\hat{R}(\theta) = e^{i\theta\hat{a}^\dagger\hat{a}}$ where θ is the rotation angle in radians. We use the following conventions for the position $\hat{q} = (\hat{a} + \hat{a}^\dagger)/2$ and the momentum $\hat{p} = i(\hat{a}^\dagger - \hat{a})/2$, in natural units of $\hbar = 1/2$.

Our schemes produce states similar to those in Eq. (1), but not exact squeezed cat states, with fidelity improving to unity as n increases. We will later detail numerical calculations of average fidelity to demonstrate their closeness to ideal states.

The ideal infinite-energy square GKP states [15] can be written as superpositions of quadrature eigenstates. Squeezed cat states serve as approximate GKP states except with only the two most important central components, in particular

$$|1_{\text{GKP}}^\Delta\rangle \propto \left|-\sqrt{\frac{\pi}{2}}, -\ln\Delta\right\rangle + \left|\sqrt{\frac{\pi}{2}}, -\ln\Delta\right\rangle, \quad (2)$$

where $\Delta \in (0, 1]$ gives $-10\log_{10}(\Delta^2)$ dB of squeezing. Example Wigner functions of single-mode optical states relevant to this work are presented in [50].

Scheme I.—Reference [23] presents a nondeterministic approach for generating squeezed cat states, as depicted in Fig. 1(a). This method involves mixing a Fock state, denoted as $|n\rangle$, with a vacuum state on a beam splitter and subsequently measuring one of the quadratures, specifically the p quadrature, using homodyne detection. The key to this technique lies in the selection of measurement outcomes that are close to zero ($m_p \sim 0$), which results in the production of an approximate squeezed two-component cat state.

Utilizing Fock states ensures consistent amplitude and positive squeezing in generated cat states, which is advantageous for breeding GKP states. However, the homodyne detection method is constrained by the need for postselection with $m_p \approx 0$, underscoring the need for an alternative measurement technique. More details on the nondeterministic preparation of large-amplitude cat states using homodyne detection are provided in [50].

Our scheme I, as presented in Fig. 1(b), addresses the limitations of previous methods by enabling the deterministic preparation of squeezed cat states from Fock states. In this scheme, a Fock state is divided among $k + 1$ paths using a $(k + 1)$ splitter, distributing approximately equal portions of the state to each of the k detectors, while the remaining part becomes the output state in the final mode. Prior to detection, each of the initial k modes undergoes

squeezing in distinct directions, followed by photon-number-resolving detection (PNRD). With a sufficiently large initial photon number n, this approach guarantees the deterministic generation of two-component squeezed cat states in the remaining mode with high fidelity. Detailed explanations and proofs concerning scheme I are presented in [50].

The generation of the squeezed cat state in our scheme is dependent upon a set of chosen parameters: the photon number n of the input Fock state, the number of modes k involved in the detection, and the orientations of squeezing θ_j. These parameters are selected by the experimenter. The prepared cat state is also dependent upon the measurement outcomes m_j at the detectors, which are the experimentally observed values. While n, k, and θ_j are predetermined, influencing the characteristics of the resulting state, the scheme deterministically produces approximate squeezed cat states, regardless of the m_j values. The orientation of the squeezed cat state is ultimately defined through a combination of these experimental choices and the outcomes of the measurements. The orientation angle of the squeezed cat state can be derived through analytical or numerical calculations.

The amplitude of the prepared cat state is given by $|\alpha| \approx \sqrt{n\eta_{\text{total}}}$. Additionally, the squeezing parameter of the cat state r can be approximated by $r \approx -0.5 \ln(1 - \eta_{\text{total}})$.

The squeezing applied to each of the $k + 1$ modes is directed along different orientations θ_j. For values of $k > 2$, the squeezing angles θ_j can be set to be equidistant around a circle, specifically, $\theta_j = j\pi/k$ where $j = 1, 2, \ldots, k$. In the case of $k = 2$, $\theta_j = j\pi/4$ can be used. For large k, $\theta_j \in [0, \pi)$ can be selected randomly.

When set to $k = 1$, the $k + 1$ splitter is simply a beam splitter. The output state always manifests as either two- or four-component cat states, dependent on the measurement outcome in the other mode. This is clearly illustrated in the first measurement stage of Fig. 1(c). For large squeezing, the components of the prepared cat state are precisely positioned at the intersections of a circle defined by $n\eta = |\alpha|^2$ and an ellipse described by $b = m\eta/(1 - \eta) = e^{2r}\text{Re}(\alpha)^2 + e^{-2r}\text{Im}(\alpha)^2$. These components are situated at angles $\{\phi_1, -\phi_1, \phi_1 + \pi, -\phi_1 + \pi\}$ where $|\phi_1|$ falls within the range $[0, \pi)$.

To prepare two-component cat states deterministically, the circuit iterates with directionally rotated squeezing relative to the initial state, as shown in the second measurement stage of Fig. 1(c). This technique isolates one pair of components from the initially prepared four-component cat state. As the initial photon number n increases, these cat components become clearly distinguishable, ensuring the production of high-fidelity two-component cat states for large n. Further details are documented in [50].

It can be beneficial to iterate the protocol more than twice ($k > 2$), applying squeezing in varying directions,

mirroring the evolution using the approach given in Fig. 1(b). This is illustrated and summarized in Fig. 1(d)(I). It is practical to maintain a constant transmissivity $\eta_j = \eta$ for all beam splitters. In this case, the total transmissivity experienced by the input state is $\eta_{\text{total}} = \eta^k$.

Scheme II.—Scheme II is introduced to address the limitations encountered in scheme I, specifically the requirements for a large n, the necessity of inline squeezing, and instances of nonunit fidelity for finite n.

First, we recognize that the phase probability distribution of any given state undergoes a similar evolution for the following specific circuits when considering a scenario of high transmissivity η:
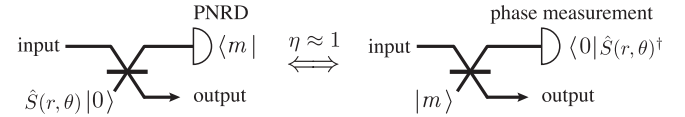
We address the absence of an experimentally feasible phase measurement, as necessitated by the right circuit. Instead, scheme II capitalizes on the availability of squeezed vacuum states, a requirement of the left circuit, which is experimentally implementable. By iteratively applying this circuit with random $\theta_j \in [0, \pi)$, scheme II effectively simulates a phase measurement, thereby enabling the deterministic preparation of cat states. This is summarized in Fig. 1(d)(II). As detailed in [50], we demonstrate that the phase probability distribution of the system gradually evolves to exhibit two distinct peaks at ϕ and $\phi + \pi$, where $\phi \in (0, \pi]$.

Scheme II allows for any input pure state with at least twofold rotational symmetry (even or odd Fock-number parity), making squeezed Fock states particularly suitable. While both schemes deterministically generate cat states in theory, scheme I requires input states with a constant amplitude n, which can be impractical in experiments due to the challenges of generating large Fock states. Conversely, scheme II can utilize more readily available squeezed Fock states. However, this introduces some nondeterminism when n is small, as not all states produced are high-fidelity large-amplitude squeezed cat states. This nondeterminism, due to the selective filtering of states, makes scheme II more adaptable and potentially more feasible for experimental use.

Squeezing is a valuable tool to exponentially enhance the achievable amplitude and mean photon number of the prepared cat states. More analysis is presented in [50].

Numerical simulations of scheme II are illustrated for two different input states in Fig. 2. The first simulation, depicted in Fig. 2(a), uses a Fock state input $|20\rangle$, and the second, shown in Fig. 2(b), utilizes a squeezed Fock state input $\hat{S}(r)|3\rangle$ with 6 dB of squeezing. In both scenarios, the total transmissivity is set to $\eta^k = 1/2$, the squeezed vacuum inputs are prepared with 6 dB of squeezing, and the process iterates over $k = 100$ rounds. The Wigner functions for the
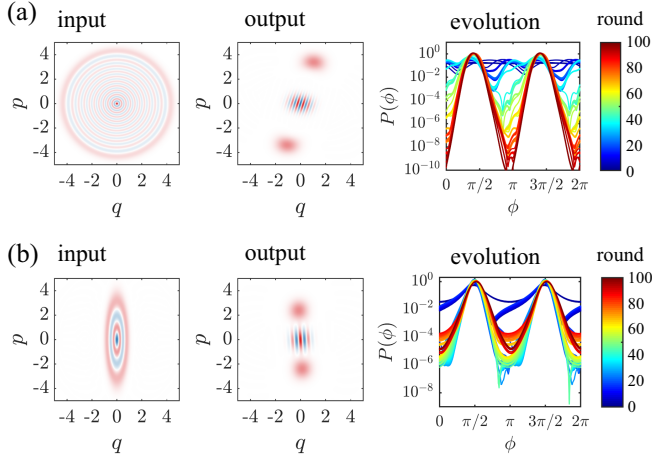
FIG. 2. Simulation results for scheme II, utilizing a total transmissivity of $\eta^k = 1/2$, with $k = 100$ rounds, and employing squeezed vacuum states with 6 dB of squeezing. The results highlight various input states, including (a) an input Fock state $|n\rangle$ where $n = 20$, and (b) an input squeezed Fock state $\hat{S}(r)|n\rangle$ with $n = 3$ and 6 dB of squeezing. For both scenarios, the Wigner functions of the input state (left), the output state (middle), and the evolution of the phase probability distribution $P(\phi)$ (right), transitioning from blue to red, are presented.

initial state (left), the final state (center), and the evolution of the phase probability distribution $P(\phi)$ (right) [56] are plotted for both simulations.

Performance and imperfections.—To evaluate the performance of our prepared squeezed cat states, we focus on two critical metrics: fidelity and squeezing, considering both ideal and nonideal detectors. Details on experimental imperfections such as dephasing, loss, detector efficiencies, optimal k, average fidelity relative to input Fock state n, and the functionality of scheme II with nonideal inputs are available in [50].

Fidelity serves as a comparative measure between the prepared output state and an ideal target cat state. Given the variability in the amplitudes, parity, and squeezing of the output states from our schemes, we first align the prepared cat state using Gaussian operations onto the GKP grid to be $\sim|1_{\text{GKP}}^{\Delta}\rangle$, as described by Eq. (2). This is an ideal configuration suitable for GKP breeding. To obtain a squeezing level for the ideal target cat state, we examine the variance in the p quadrature of the prepared cat state.

The anticipated squeezing for the adjusted prepared squeezed cat state [in the form of Eq. (2)] can be calculated using the formula [50]

$$\Delta = \sqrt{\pi(1 - \eta^k)/(2n\eta^k)}. \tag{3}$$

In Fig. 3, we present the performance of our prepared cat states. (a) illustrates the average fidelity of the prepared cat states relative to the target cat state. (b) displays the average squeezing achieved by the cat states. The results are
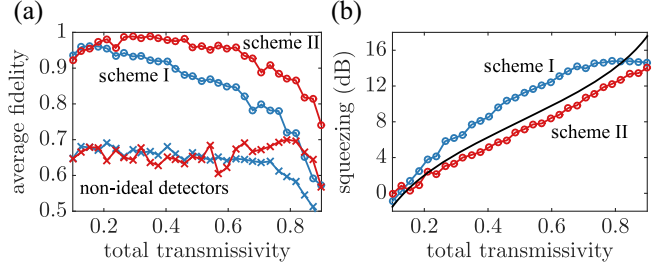
FIG. 3. Performance of deterministically prepared squeezed cat states utilizing scheme I (blue) and scheme II (red), for an input Fock state with $n = 10$ displaying fidelity in (a), assuming ideal detectors (circle markers) and inefficient detectors (cross markers) with an efficiency of $\epsilon = 0.98$, and squeezing in (b), assuming ideal detectors (circle markers). The results are averaged over 100 simulations. For scheme I, the configuration includes $k = 10$ rounds and 6 dB of inline squeezing. For scheme II, $k = 100$ rounds are applied when using ideal detectors, whereas $k = 10$ rounds for nonideal detectors, with both situations involving a squeezed vacuum subjected to 6 dB of squeezing. Additionally in (b), the expected analytical squeezing (black) is plotted as per Eq. (3).

evaluated as a function of total transmissivity η^k for an input Fock state where $n = 10$, showcasing the results for scheme I (blue) and scheme II (red), averaged over 100 experimental runs. These scenarios utilize either ideal detectors (circle markers), or nonideal detectors (cross markers) with a detection efficiency of $\epsilon = 0.98$, which is experimentally achievable [32]. Additionally, the expected squeezing, as derived from Eq. (3), is plotted (black) for comparison. For scheme I, parameters include a total of $k = 10$ rounds and 6 dB of inline squeezing. In contrast, scheme II is executed over $k = 100$ iterations when employing ideal detectors and adjusted to $k = 10$ iterations for nonideal detectors, a modification intended to mitigate the impact of detection noise, and the squeezed vacuum is subjected to 6 dB of squeezing.

The results reveal a trade-off between fidelity and squeezing. Notably, these results can be enhanced through the selective postprocessing of the outputs, focusing on the highest quality cat states generated during the experimental runs.

We estimate a good practical value of k required to achieve a good fidelity in experiment for both scheme I and scheme II for $n = 10$ assuming detector efficiency of 98% is between 4 and 10. For plots showing how the average fidelity behaves with k, see Ref. [50].

GKP error correction.—Before GKP states can be deterministically prepared through breeding [41–43], the prepared cat states must first be adjusted into the form given by Eq. (2).

Equation (3) establishes a relationship between n and Δ for a given total transmissivity η^k. By setting $\eta^k = 1/2$, it is observed that as n increases, the squeezing becomes large, and the fidelity approaches unity, i.e., $\lim_{n \to \infty} \Delta = 0$ and

$\lim_{n\to\infty} F = 1$. High fidelity for large n is attributed to the reduction of phase uncertainty in the effective phase measurements performed. Consequently, approximate GKP states can be prepared with exceptionally high quality, characterized by both fidelity and squeezing. This enables the possibility of fault-tolerant quantum computation utilizing GKP error correction, using our schemes for state preparation.

In [50], we explore how the quantum states prepared via our schemes perform in the context of GKP error correction.

Conclusions.—In this Letter, we have introduced methods for the deterministic preparation of squeezed cat states in optics. These methods hinge on the availability of large Fock states or states with even (or odd) parity, the use of PNRDs, and the application of Gaussian measurements and operations. Together, these components can achieve universal fault-tolerant quantum computation and long-distance quantum communication through GKP error correction.

Incorporating feed-forward mechanisms can significantly enhance our schemes by enabling dynamic adjustments. This could include modifying beam splitter transmissivities or adjusting squeezing angles and magnitudes to optimize state preparation based on initial measurement outcomes.

We hope that our findings will allow experimental advancements in quantum information processing and error correction, particularly with the use of squeezed cat and GKP states.

[*] mattwinnel@gmail.com

[1] F. Arute *et al.*, Nature (London) **574**, 505 (2019).

[2] V. Scarani, H. Bechmann-Pasquinucci, N. J. Cerf, M. Dušek, N. Lütkenhaus, and M. Peev, Rev. Mod. Phys. **81**, 1301 (2009).

[3] D. Gottesman, *An Introduction to Quantum Error Correction and Fault-Tolerant Quantum Computation* (2009), https://redirect.cs.umbc.edu/~lomonaco/ams2009-talks/Gottesman-Paper.pdf.

[4] S. L. Braunstein and P. van Loock, Rev. Mod. Phys. **77**, 513 (2005).

[5] H. Yonezawa and A. Furusawa, Opt. Spectrosc. **108**, 288 (2008).

[6] N. Cerf, G. Leuchs, and E. Polzik, *Quantum Information With Continuous Variables of Atoms And Light* (World Scientific Publishing Company, Singapore, 2007).

[7] C. Weedbrook, S. Pirandola, R. García-Patrón, N. J. Cerf, T. C. Ralph, J. H. Shapiro, and S. Lloyd, Rev. Mod. Phys. **84**, 621 (2012).

[8] A. Serafini, *Quantum Continuous Variables: A Primer of Theoretical Methods* (CRC Press, Boca Raton, 2017), 10.1201/9781315118727.

[9] M. Mirrahimi, Z. Leghtas, V. V. Albert, S. Touzard, R. J. Schoelkopf, L. Jiang, and M. H. Devoret, New J. Phys. **16**, 045014 (2014).

[10] M. Bergmann and P. van Loock, Phys. Rev. A **94**, 042332 (2016).

[11] L. Li, C.-L. Zou, V. V. Albert, S. Muralidharan, S. M. Girvin, and L. Jiang, Phys. Rev. Lett. **119**, 030502 (2017).

[12] Q. Xu, G. Zheng, Y.-X. Wang, P. Zoller, A. A. Clerk, and L. Jiang, npj Quantum Inf. **9**, 78 (2023).

[13] D. S. Schlegel, F. Minganti, and V. Savona, Phys. Rev. A **106**, 022431 (2022).

[14] H. Le Jeannic, A. Cavaillès, K. Huang, R. Filip, and J. Laurat, Phys. Rev. Lett. **120**, 073603 (2018).

[15] D. Gottesman, A. Kitaev, and J. Preskill, Phys. Rev. A **64**, 012310 (2001).

[16] D. V. Sychev, A. E. Ulanov, A. A. Pushkina, I. A. Fedorov, M. W. Richards, P. Grangier, and A. I. Lvovsky, AIP Conf. Proc. **1936**, 020018 (2018).

[17] D. V. Sychev, A. E. Ulanov, A. A. Pushkina, M. W. Richards, I. A. Fedorov, and A. I. Lvovsky, Nat. Photonics **11**, 379 (2017).

[18] M. Dakna, T. Anhut, T. Opatrný, L. Knöll, and D.-G. Welsch, Phys. Rev. A **55**, 3184 (1997).

[19] J. Etesse, M. Bouillard, B. Kanseri, and R. Tualle-Brouri, Phys. Rev. Lett. **114**, 193602 (2015).

[20] M. Endo, R. He, T. Sonoyama, K. Takahashi, T. Kashiwazaki, T. Umeki, S. Takasu, K. Hattori, D. Fukuda, K. Fukui, K. Takase, W. Asavanant, P. Marek, R. Filip, and A. Furusawa, Opt. Express **31**, 12865 (2023).

[21] Z. Zhang, L. Shao, W. Lu, and X. Wang, Phys. Rev. A **106**, 043721 (2022).

[22] R. Dahan, G. Baranes, A. Gorlach, R. Ruimy, N. Rivera, and I. Kaminer, Phys. Rev. X **13**, 031001 (2023).

[23] A. Ourjoumtsev, H. Jeong, R. Tualle-Brouri, and P. Grangier, Nature (London) **448**, 784 (2007).

[24] K. Takase, J. I. Yoshikawa, W. Asavanant, M. Endo, and A. Furusawa, Phys. Rev. A **103**, 013710 (2021).

[25] T. Gerrits, S. Glancy, T. S. Clement, B. Calkins, A. E. Lita, A. J. Miller, A. L. Migdall, S. W. Nam, R. P. Mirin, and E. Knill, Phys. Rev. A **82**, 031802(R) (2010).

[26] K. Takase, K. Fukui, A. Kawasaki, W. Asavanant, M. Endo, J.-i. Yoshikawa, P. van Loock, and A. Furusawa, arXiv:2212.05436.

[27] M. S. Podoshvedov, S. A. Podoshvedov, and S. P. Kulik, arXiv:2212.08827.

[28] M. Eaton, C. Gonzá lez-Arciniegas, R. N. Alexander, N. C. Menicucci, and O. Pfister, Quantum **6**, 769 (2022).

[29] J. Provazník, L. Lachman, R. Filip, and P. Marek, Opt. Express **28**, 14839 (2020).

[30] T. Gerrits, B. Calkins, N. Tomlin, A. E. Lita, A. Migdall, R. Mirin, and S. W. Nam, Opt. Express **20**, 23798 (2012).

[31] A. E. Lita, A. J. Miller, and S. W. Nam, Opt. Express **16**, 3032 (2008).

[32] D. Fukuda, G. Fujii, T. Numata, K. Amemiya, A. Yoshizawa, H. Tsuchida, H. Fujino, H. Ishii, T. Itatani, S. Inoue, and T. Zama, Opt. Express **19**, 870 (2011).

[33] N. Sridhar, R. Shahrokhshahi, A. J. Miller, B. Calkins, T. Gerrits, A. Lita, S. W. Nam, and O. Pfister, J. Opt. Soc. Am. B **31**, B34 (2014).

[34] K. Xia, G. K. Brennen, D. Ellinas, and J. Twamley, Opt. Express **20**, 27198 (2012).

[35] M. Uria, P. Solano, and C. Hermann-Avigliano, Phys. Rev. Lett. **125**, 093603 (2020).

[36] J. E. Bourassa, R. N. Alexander, M. Vasmer, A. Patil, I. Tzitrin, T. Matsuura, D. Su, B. Q. Baragiola, S. Guha, G. Dauphinais, K. K. Sabapathy, N. C. Menicucci, and I. Dhand, Quantum **5**, 392 (2021).

[37] K. K. Sabapathy, H. Qi, J. Izaac, and C. Weedbrook, Phys. Rev. A **100**, 012326 (2019).

[38] D. Su, C. R. Myers, and K. K. Sabapathy, Phys. Rev. A **100**, 052301 (2019).

[39] N. Quesada, L. G. Helt, J. Izaac, J. M. Arrazola, R. Shahrokhshahi, C. R. Myers, and K. K. Sabapathy, Phys. Rev. A **100**, 022341 (2019).

[40] I. Tzitrin, J. E. Bourassa, N. C. Menicucci, and K. K. Sabapathy, Phys. Rev. A **101**, 032315 (2020).

[41] H. M. Vasconcelos, L. Sanz, and S. Glancy, Opt. Lett. **35**, 3261 (2010).

[42] D. J. Weigand and B. M. Terhal, Phys. Rev. A **97**, 022341 (2018).

[43] S. C. Policarpo and H. M. Vasconcelos, Braz. J. Phys. **46**, 294 (2016).

[44] B. Q. Baragiola, G. Pantaleoni, R. N. Alexander, A. Karanjai, and N. C. Menicucci, Phys. Rev. Lett. **123**, 200502 (2019).

[45] S. Konno, W. Asavanant, F. Hanamura, H. Nagayoshi, K. Fukui, A. Sakaguchi, R. Ide, F. China, M. Yabuno, S. Miki, H. Terai, K. Takase, M. Endo, P. Marek, R. Filip, P. van Loock, and A. Furusawa, Science **383**, 6680 (2024).

[46] Matlab, The Mathworks, Inc., Natick, Massachusetts.

[47] N. Killoran, J. Izaac, N. Quesada, V. Bergholm, M. Amy, and C. Weedbrook, Quantum **3**, 129 (2019).

[48] https://github.com/mattwinnel/catprep.git.

[49] https://github.com/JGuanzon/cat-preparation.

[50] See Supplemental Material at http://link.aps.org/supplemental/10.1103/PhysRevLett.132.230602 for more Wigner function plots, derivations, proofs, results including experimental imperfections, and performance for GKP error correction; and for extended analyses and simulations, which includes Refs. [51–55].

[51] J. Janszky, P. Domokos, and P. Adam, Phys. Rev. A **48**, 2213 (1993).

[52] J. J. Gong and P. K. Aravind, Am. J. Phys. **58**, 1003 (1990).

[53] A. L. Grimsmo, J. Combes, and B. Q. Baragiola, Phys. Rev. X **10**, 011058 (2020).

[54] M. Grant and S. Boyd, CVX: Matlab software for disciplined convex programming, version 2.1, http://cvxr.com/cvx (2014).

[55] V. V. Albert, K. Noh, K. Duivenvoorden, D. J. Young, R. T. Brierley, P. Reinhold, C. Vuillot, L. Li, C. Shen, S. M. Girvin, B. M. Terhal, and L. Jiang, Phys. Rev. A **97**, 032346 (2018).

[56] H. M. Wiseman and R. B. Killip, Phys. Rev. A **57**, 2169 (1998).